LANGMUIR

Biological and Environmental Phenomena at the Interface

Investigation of Electromagnetic Resonance Rewarming Enhanced by Magnetic Nanoparticles for Cryopreservation

Jiaji Pan, Shen Ren, Praveen KaliappanSekar, Ji Peng, Zhiquan Andy Shu, Gang Zhao, Weiping Ding, Ming Chen, and Dayong Gao

Langmuir, **Just Accepted Manuscript** • DOI: 10.1021/acs.langmuir.8b03060 • Publication Date (Web): 14 Dec 2018

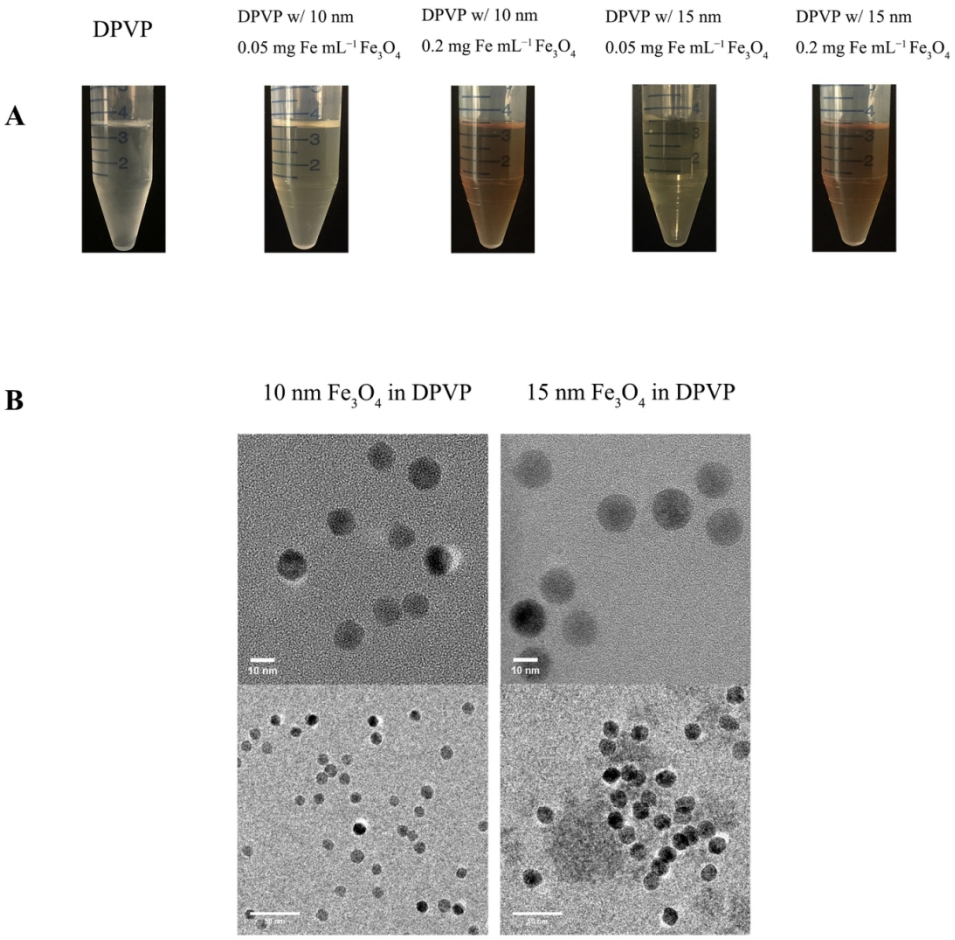

DPVP solutions with 10, 15nm Fe3O4 nanoparticles: (A) visual examination of solutions w/ or w/o different Fe3O4 concentrations after slow cooling and rapid rewarming; (B) transmission electron microscopy images. Stratified solution after rewarming or nanoparticle aggregations were not observed.

119x119mm (300 x 300 DPI)

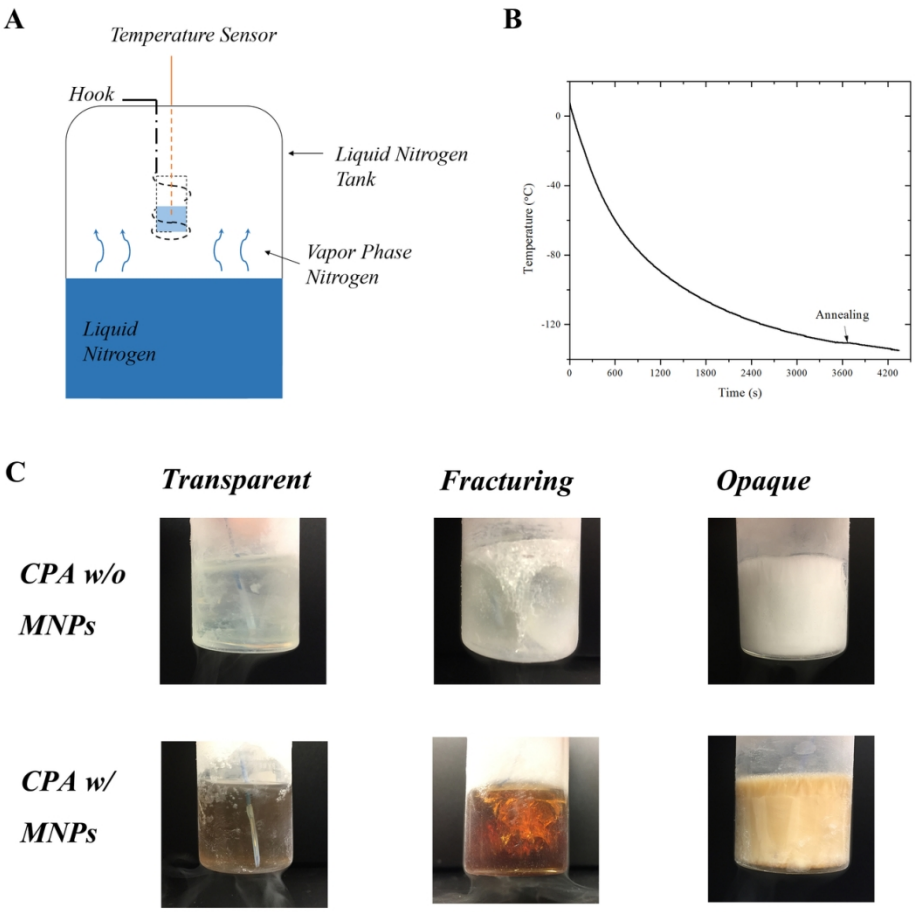

(A) Schematic illustration of the controlled cooling setup. The CPA solutions in holder is hanged by a hook and placed above the surface of liquid nitrogen. The cooling rate could be roughly estimated by adjusting the distance between the CPA and the liquid nitrogen level. (B) A representative temperature change is illustrated using this vapor phase cooling method recorded by thermal sensors. (C) Typical visual images of CPA solutions cooled down to −140 □C. DPVP w/ or w/o Fe3O4 nanoparticles formed transparent solid (left) using the vapor phase cooling method. Cracks (middle) were seen after plunging the bulk DPVP w/ or w/o nanoparticles into liquid nitrogen. Opaque crystalline solid (right) was observed for slowly cooled 5.2 M DMSO, 5.2 M DMSO solution is unable to be vitrified at this low cooling rate.

119x119mm (300 x 300 DPI)

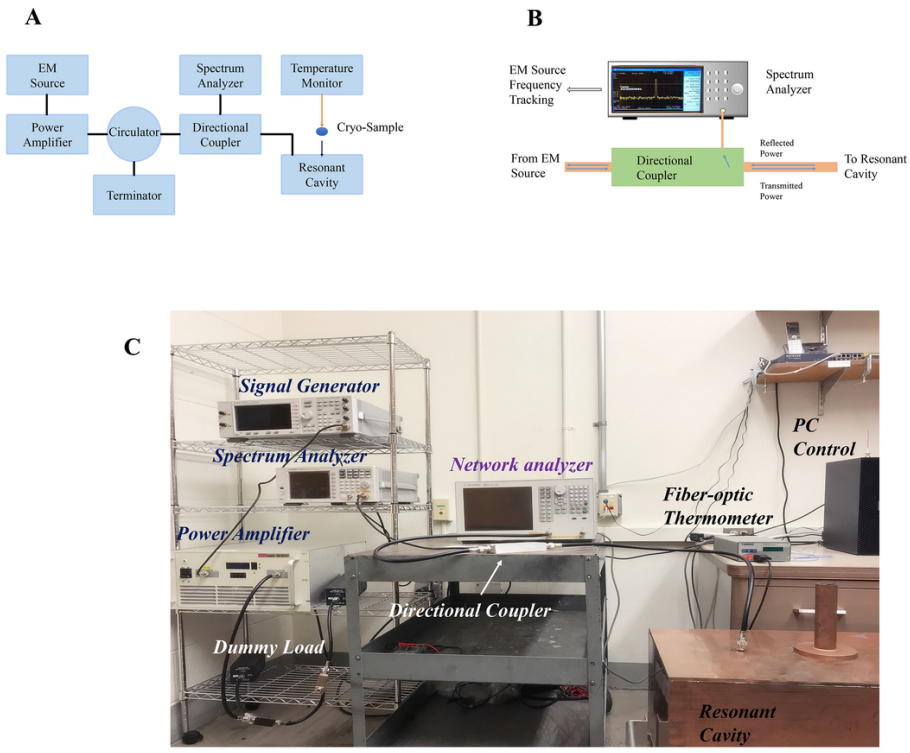

Schematic illustration (A) and photograph (C) of the entire optimized EM resonance system configuration used to achieve the ultrafast rewarming process. The dynamic feedback component (B) consists of a directional coupler and a spectrum analyzer to monitor the reflected power distribution. The EM source can be adjusted based on the acquired reflected power spectrum accordingly to track the resonance of the EM system.

97x82mm (300 x 300 DPI)

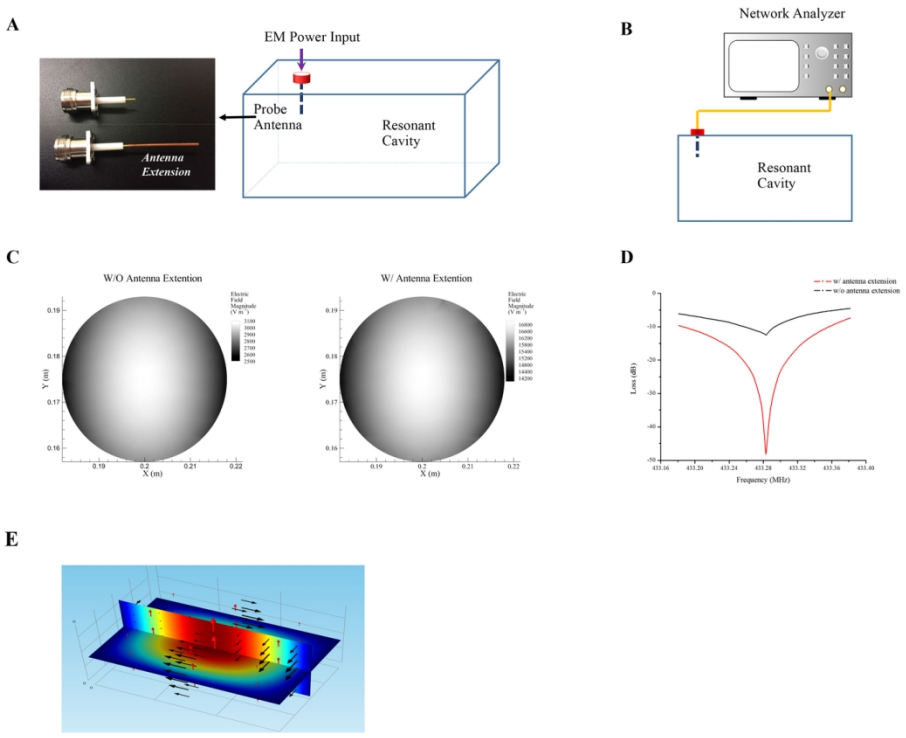

(A) Probe antenna conducting EM energy into the resonance chamber. (B) Schematic of the determination of the cavity resonance state using a network analyzer. After the addition of copper extension, a five-fold increase in the simulated electric field magnitude was seen in the center of chamber (C) where the cryopreserved material was located; the experimentally determined reflection coefficient (D) was minimized indicating much less portion of energy reflected from the resonant cavity back to the source. (E) EM field distribution inside the resonant cavity. Color slices represent the electric field magnitude. Red arrow and black arrows indicate the direction of electric and magnetic fields, respectively.

129x101mm (300 x 300 DPI)

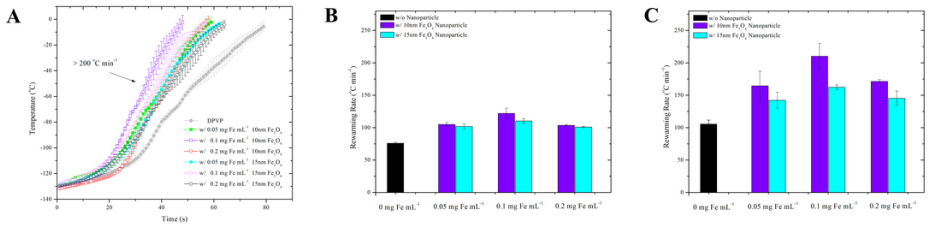

The rewarming of CPA solutions with embedded Fe3O4 nanoparticles using the EM resonance system. (A) Temperature change of the CPA solutions during the rewarming process. Average value of temperature versus time was given based on four measurements. Average warming rates were determined for the rewarming temperature range −130 ☐C to −70 ☐C (B) and −70 ☐C to 0 ☐C (C). The error bars represented the standard deviation. Each test was repeated for four times.

49x14mm (600 x 600 DPI)

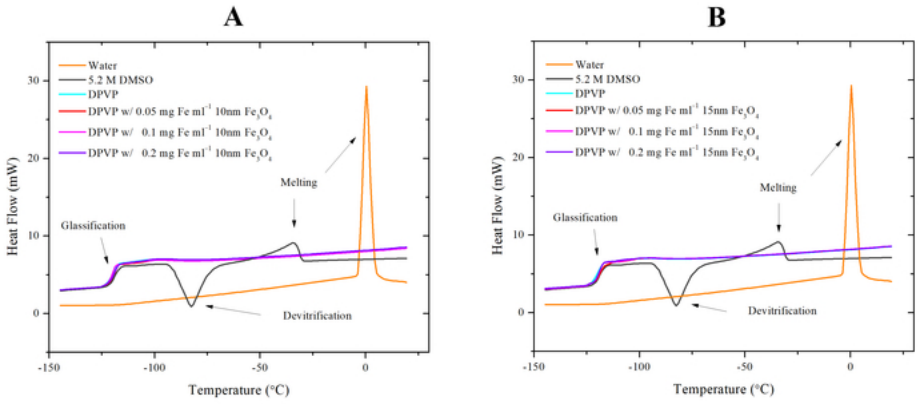

Freeze-warming behavior of CPA solutions with 10nm Fe3O4 nanoparticles (A) and 15nm Fe3O4 nanoparticles (B). The devitrification, melting of 5.2 M dimethyl sulfoxide (DMSO) occurred at a warming rate 100 □C min−1. Whereas the apparent recrystallization of DPVP with Fe3O4 nanoparticles was not observed using the same protocol. The cooling and heating rates were set in accordance with the bulk cryopreserved materials in the EM resonance rewarming.

31x13mm (600 x 600 DPI)

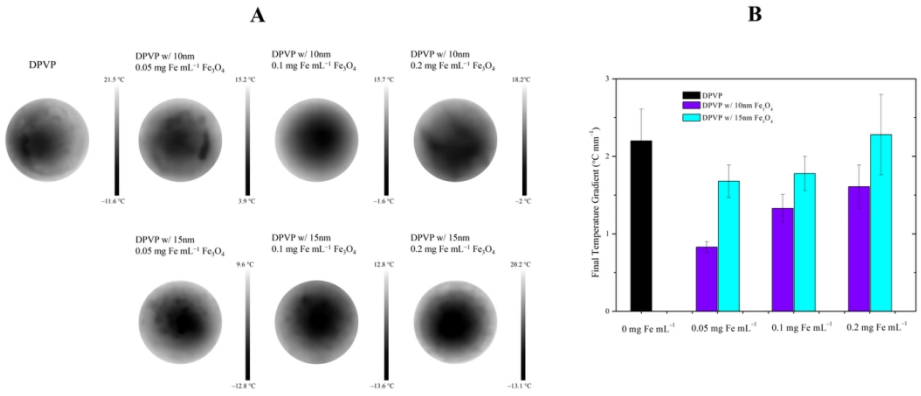

The post-rewarming of CPA solutions with embedded Fe3O4 nanoparticles using the EM resonance system. (A) Surface temperature distribution. (B) The temperature gradients were calculated as the maximum temperature difference divided by the distance. Mean values ± standard deviations were determined based on four measurements.

64x25mm (600 x 600 DPI)

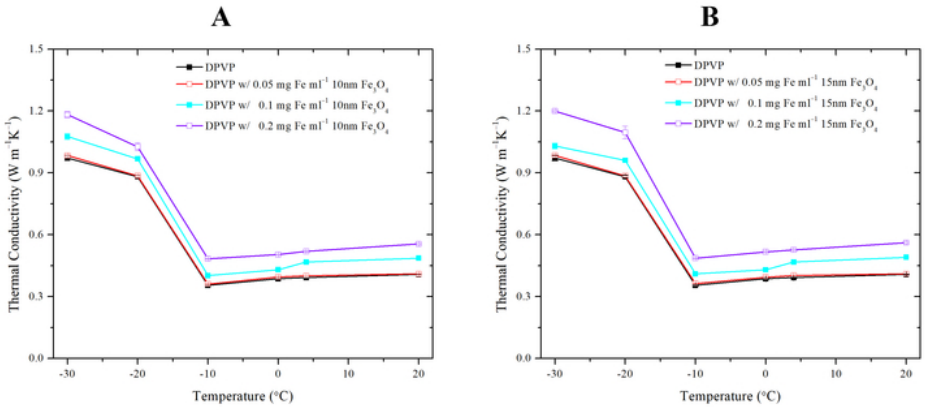

Thermal conductivities of CPA solution with 10nm Fe3O4 nanoparticles (A) and 15nm Fe3O4 nanoparticles (B). Mean values ± standard deviations were determined based on four measurements.

32x14mm (600 x 600 DPI)

Investigation of Electromagnetic Resonance Rewarming Enhanced by Magnetic Nanoparticles for Cryopreservation

*Jiaji Pan[a,b], Shen Ren[a], Praveen K. Sekar[a], Ji Peng[a], Zhiquan Shu[a,c], Gang Zhao[d], Weiping Ding[d], Ming Chen[a], and Dayong Gao[a,]**

a Center for Cryo-Biomedical Engineering and Artificial Organs, Department of Mechanical Engineering, University of Washington, Seattle, WA 98195

b School of Engineering and Design, Hunan Normal University, Changsha, China 410081

c School of Mechanical and Materials Engineering, Washington State University, Everett, WA 98201

d Department of Electronic Science and Technology, University of Science and Technology of China, Anhui 230027, China

KEYWORDS: Cryopreservation, vitrification, electromagnetic resonance rewarming, magnetic nanoparticle, thermal analysis

* Corresponding Author: Prof. Dr. Dayong Gao
TEL: +1(206)5431411. FAX: +1(206)6858047. Email: dayong@u.washington.edu

ABSTRACT

The lack of effective rewarming technique restricted the successful cryopreservation of organ or large tissues by vitrification. The conversion of electromagnetic (EM) energy into heat provides a possible solution for the rewarming process for the cryopreservation. In this work, an EM resonance rewarming system was set up with dynamic feedback control and power feeding optimization. In addition, we take advantage of magnetic nanoparticles (MNPs) to absorb magnetic field energy to further enhance the energy conversion efficiency. We achieved over 200 °C min^{-1} rewarming rate for tens of mL cryopreserved samples. Besides, we also investigated the effect of nanoparticle size and concentration based on thermal properties analyzing the contribution of nanoparticles and utilization of field energy. The closed system reduced the possible concomitant side effects when increasing nanoparticles or raising EM source power. With the remarkably low dosage of nanoparticles (0.1 mg mL^{-1} Fe) compared to other MNP based rewarming applications, this study opens a door for new approaches to explore novel techniques for the tissue and organ preservation.

Introduction

Over the past decades, magnetic nanoparticles (MNPs) have played a significant role in various diagnosis and therapeutic practices including non-invasive magnetic resonance imaging (MRI), drug delivery, and hyperthermia therapy[1, 2, 3, 4, 5, 6]. By harnessing the heating effects of MNPs under the external strong oscillating magnetic field, MNPs-based hyperthermia may achieve a selective and effective localized temperature rising intolerable to cancerous cells but less lethal to normal cells, while other cancer treatment methods may have difficulty in solely targeting specific cancerous area. Recently, the combination of radiofrequency electromagnetic system generating alternating magnetic and MNPs as thermal meditators was applied from hyperthermia into another thriving biomedical field, cryopreservation[7, 8], attempting to address the unmet need for transplantation due to tissue and organ shortage[9].

Cryopreservation, using low temperature to preserve biomaterials, serves as an important role facilitating biomedical research and clinical treatment. Currently the major progress in cryopreservation is confined to simple and/or small volume biomaterials such as red blood cells[10], stem cells[11], sperms[12] and oocytes[13]. Albeit the successful preservation may considerably alleviate the waiting for transplantation and allow for sufficient time in donor-recipient matching, complex and larger tissues/organs exhibit much more problems in establishing mature preservation methods. Vitrification, forming amorphous state by fast cooling and adding high concentration cryoprotective agents (CPA), showed its promising future for organ preservation[14]. Yet the perilous devitrification and/or thermal induced fracturing can hardly be eliminated during the rewarming process from the low storage temperature (typically −80 °C or −196 °C) to physiologically normal temperature.

The lack of rapid and uniform rewarming techniques has limited the development of tissue and organ cryopreservation for a long time. By vibrating the electrical dipole molecules, high power electromagnetic (EM) cavity heating systems[15, 16] can generate a volumetric dielectric heating and overcome the problem of low thermal conductivity and high specific heat of biological materials, which rules out the possibility of using traditional water bath for thawing large cryopreserved samples. However, the associated "thermal runaway" problem[17], temperature difference growing due to temperature dependent EM power absorption ability, hindered these multimode or unstable resonant EM systems with inadequate control to obtain an effective rewarming protocol.

The recent "nanowarming" method[8], i.e., an MNPs-based heating technique, utilized the oscillating magnetic field generated by a commercially available radiofrequency (RF) EM coil system, provided an impressive solution for the large tissue (over 1 mL to tens of mL) cryopreservation. But a few concerns remain. The heat generation inside the cryopreserved material mainly relies on the ability of embedded MNPs to convert magnetic field energy into heat. Whereas cytotoxicity of MNPs reported in specific types of cells[18, 19] should be noted. For organs or more complex tissues where cellular uptake of nanoparticles could take place[20], high dosage of MNPs in organs may result in undesired side effects. On the other hand, the increasing technical difficulty to enlarge RF power[21], an inevitable obstacle due to the relatively low energy utilization efficiency, may inhibit the system scaling up to organ preservation.

In this study, to achieve high energy conversion efficiency as well as minimize the dosage of MNPs, a dynamically controlled EM resonance rewarming system was set up and optimized. To utilize both electric field and magnetic field energy, 10nm or 15nm iron oxide nanoparticles at different low concentrations were incorporated in the CPA solutions rewarmed by the optimized rewarming system for the proof of concept purpose. The average highest warming rate (over 200

°C min^{-1}) for bulk cryopreserved material was achieved using smaller EM power compared to the RF coil magnetic rewarming or suboptimal EM systems. The post-rewarming temperature distribution was determined, and thermal analyses were conducted to investigate the enhanced effects brought by the nanoparticles. The optimum amount of nanoparticles required was largely reduced (0.1 mg Fe mL^{-1}) for the rapid and uniform rewarming by using this optimized EM resonance rewarming system, which will pose less side effects for the subsequent biological trials compared to over 1 mg Fe mL^{-1} in other rewarming techniques[7, 8, 22]. With the great decrement of MNPs dosage and enhanced heating efficiency, this preliminary study points to a promising alternative strategy to deal with the rewarming problem towards tissue and organ preservation.

Experimental details

CPA/vitrification solution

DPVP contains 5.2 M dimethyl sulfoxide (DMSO; Sigma-Aldrich, St. Louis, MI, USA), 6% (g/dl) polyvinylpyrrolidone (PVP; Sigma-Aldrich) in PBS (Sigma-Aldrich) solution of which the dielectric properties were measured in our previous work and presumed to be able to reduce the thermal runaway phenomenon[23]. 5 M DMSO solution was used as comparison in the freezing/vitrifying examination. Solutions were prepared the day before the cooling and rewarming experiments.

Magnetic nanoparticles

The MNPs used in this study were 10, 15nm iron oxide nanoparticles (Fe_3O_4) with amine group dissolved in 10 mM PBS (Ocean NanoTech LLC, San Diego, CA, USA). After diluting MNPs solution in the CPA solutions, the composite of CPA solution with MNPs achieved low concentrations of 0.05, 0.1, 0.2 mg Fe mL^{-1} respectively for DPVP solutions. The distribution of

MNPs of two different sizes in the DPVP solutions were examined with transmission electron microscopy (TEM, FEI TECNAI F20 electron microscope operating at 200kV). DPVP with embedded MNPs droplets were casted onto either 200 mesh carbon coated grids or 300 mesh lacey carbon grids (Electron Microscopy Sciences, Hatfield, PA, USA). Imaged with a Gatan Ultrascan CCD using Digital Micrograph software (Gatan, Pleasanton, CA, USA).

Bulk sample cooling/vitrifying process

The bulk CPA solutions (20 mL in 30 mm × 100 mm holder) were held by an aluminum hook, placed in a liquid nitrogen container above the liquid level, and cooled by the vapor phase nitrogen as illustrated in Fig. 2A. The temperature change of the CPA solutions was recorded, and the cooling rate was estimated for the following thermal analysis. After reaching −140 °C, the CPA solutions were observed to check if the transparent amorphous state or opaque crystalline solid state was achieved.

Dynamically controlled EM resonance rewarming system

The high precision signal generator (Keysight Technologies, Santa Rosa, CA, USA) and an RF amplifier (OPHIR RF, Los Angeles, CA, USA) were combined to initiate a precise and continuous EM signal with theoretically maximum 600W power. The EM energy was conducted to a cavity with dimension determined previously [24] by coaxial cables, of which the length was minimized to reduce EM energy dissipation in line. Provided with around 430 MHz initiated EM signal, the resonance state of the cavity was excited. A standing wave pattern of alternating electric field and coupled circular oscillating magnetic field was established. During the rewarming process, the resonant frequency of the cavity loaded with cryopreserved materials changed according to the temperature dependent properties of the cryopreserved materials. A dynamic resonance tracking component was adapted to optimize the efficiency of the EM rewarming system. In this dynamic

control component, a spectrum analyzer (Keysight Technologies, Santa Rosa, CA, USA) was employed to examine the reflection status of a wide frequency spectrum. The spectrum analyzer demonstrated the distribution of reflected power versus frequency dynamically during the rewarming process. The frequency at the peak in the spectrum corresponded to the resonant state to be tracked with. The peak of the spectrum was located by the inherent function of the spectrum analyzer continuously. The frequency at the peak of the spectrum was transmitted and the signal frequency was changed according to this feedback spectrum information, maintaining a high power utilization fraction.

Extended probe antenna and effect evaluation

The probe antenna (Amphenol RF, Danbury, CT, USA) was one of the key parts to deliver EM power from the source into the chamber to set up the resonance for rapid rewarming. Additionally, a copper extension was drilled and connected to the antenna with high electrical conductive glue (Parker Hannifin, Cleveland, OH, USA).

The resonance state of the system with or without the probe antenna extension was determined from reflection signal S_{11} with a network analyzer (Keysight Technologies, Santa Rosa, CA, USA). Reflection signal represents the ratio of reflected power to total EM power. A higher reflection rate implies lower portion of EM power remains in the system, thus reducing the available power conversion for the rewarming. The simulation of the electric field magnitude within the cryopreserved material also showed the difference of electromagnetic field magnitude which provides the major heating source.

Temperature profile measurement

In order to avoid interfering the established EM field distribution, fiber optic sensors connected to a thermometer (Neoptix, Quebec city, QC, Canada) were inserted into the CPA solutions to

record real-time temperature during the rewarming process. When the cryopreserved CPA solutions reached 0 °C (i.e. passed the lethal temperature zone −60 °C to −5 °C[25], or devitrification/recrystallization zone), an infrared thermal camera (FLIR, Wilsonville, OR, USA) was used to take thermography of the surface of the CPA solutions.

Characterization of the freezing-thawing behavior

Differential scanning calorimetry measurements (DSC; Perkin Elmer, Waltham, MA, USA) were conducted to determine the freezing-thawing behavior and specific heat of the sample solution with different concentrations of MNPs. An empty pan was used as reference. Calibrations of temperature, heat flow were conducted before the measurements using n-dodecance and n-octane. 6 μL of each sample solution was placed and sealed in aluminum pans and transferred into DSC for measurements. All measurements were replicated for three times. For the analysis of freezing-thawing behavior, the samples were cooled down to −150 °C at 5 °C min^{-1} followed by heating up to 20 °C at 100 °C min^{-1}.

Thermal conductivity assessment

The thermal conductivity measurement system for CPA solutions developed by Liang *et al*[26] consists of a digital multimeter (Keithley, Cleveland, OH, USA), a microfabricated thermal sensor and a computer for data acquisition. The sensor works with the principle of transient hot wire . This miniaturized device adopted a SiO_2/Au/SiO_2 sandwiched structure to protect the microfabricated integrated heater and passive thermometer. The sensor has already been tested and shown to measure thermal conductivity of biomaterials and solutions with high accuracy, repeatability and reliability. All measurements were performed for three times from −30 to 20 °C.

Statistical analysis

The statistical analysis was carried out using R (version 3.4.2). The data were presented as mean value ± standard deviation. Differences of $p < 0.05$ were considered to be of statistical significance.

Results and Discussions

CPA solutions embedded with MNPs

Fe_3O_4 were incorporated into the DPVP solutions (41% dimethyl sulfoxide (DMSO), 6% polyvinylpyrrolidone) to make use of the magnetic field component in this EM resonance system aiming to improve the rewarming results. Fig. 1A shows the CPA solutions with 10 nm or 15 nm iron oxide nanoparticles at 0, 0.05, 0.2 mg Fe mL^{-1}, respectively. All these solutions went through freezing process down to −80 °C, storage at the −80 °C freezer for at least one day and the following thawing process. There were no visible nanoparticle clusters or solution stratification which occurred elsewhere in other CPA solutions after adding iron oxide nanoparticles[8]. The mitigation of cluster effect may be due to the lower concentration nanoparticles we used. For the MNP-based RF heating biomedical applications, it was reported that the aggregation of nanoparticles hindered the ability to convert EM energies[27], which should be avoided to obtain an efficient magnetic heat induction. The TEM images (Fig. 1B) demonstrate that the nanoparticles were dispersed without significant aggregations at the low concentrations used in this work, which may be desired to interact with the electromagnetic field. The potential unexpected inhomogeneity due to large nanoparticle aggregation could also be mitigated in the EM rewarming.

To achieve vitrification of the CPA solutions, controlled slow cooling procedures were performed using the designed cooling device (Fig. 2A). The critical cooling rate (CCR; the necessary cooling rate above which to avoid noticeable ice formation)[28] for DPVP[29] was below 5°C min^{-1}. Fig. 2B shows a typical temperature change for DPVP during the cooling process. The

cooling was slow but at a higher rate than the CCR. As Fig. 2C shows, transparent solids were formed at −140 °C by this vapor phase nitrogen cooling for every DPVP solutions with nanoparticles at different concentrations in the current study. Instead, opaque crystalline solids were observed, if the relatively lower concentration CPAs (41%, i.e., 5.2 M DMSO was used here) were slowly cooled down to −140 °C. Often, the vitrification of small volume cryopreserved biomaterial requires ultra-rapid cooling achieved by direct immersion into liquid nitrogen[30, 31]. However, it is extremely difficult to cool a bulk cryopreserved material both rapidly and uniformly. Non-uniform temperature profile associated with rapid cooling can induce mechanical stresses and cracks for bulk cryopreserved materials. As can be seen in Fig. 2C, substantial ice crystals were observed around the fracture planes in the CPA solutions plunged into liquid nitrogen rather than cooled by vapor phase nitrogen avoiding the cracks otherwise.

Optimization of the EM resonance rewarming system

The presented EM resonance rewarming system (Fig. 3A and C) established a standing wave pattern EM field inside the rewarming chamber. Under the circumstance in absence of MNPs, the heat generation is due to the dipole molecules vibrated by the strong oscillating electric field in the resonant cavity which only remains stable at the resonant state, and can be continuously altered by the cryopreserved materials inside at different temperatures. Hence, maintaining the resonance state during the entire rewarming is needed for ultrafast rewarming. Unlike commercial microwave oven using magnetron with shifting frequency (2450 ± 50 MHz), the EM source in this system is stable to avoid undesired termination of resonance state (i.e., the mismatch between the generated EM source and the cavity resonant frequency). The feedback tracking of the resonance state was realized by using a spectrum analyzer to monitor the entire reflected power-frequency distribution

(Fig. 3B). During the rewarming process, the resonance state inside the heating cavity was maintained by EM source adjustment based on the obtained spectrum feedback.

The probe antenna (Fig. 4A) that conducted EM energy from the source into the resonant chamber was optimized before the rewarming experiment. The length of the probe antenna was extended to achieve a finer coupling between the resonant chamber and EM source. As numerical simulation results (Fig. 4C) demonstrate, the extended antenna led to almost five-fold increase of the magnitude of electric field in the center area of the cavity where cryopreserved sample was rewarmed, implying more rapid warming could be realized. Then we attached a copper extension part to the original antenna and experimentally compared the EM reflection response of the cavity with or without the copper extension by using a network analyzer (Fig. 4B). Fig. 4D shows the experimental test results of reflection coefficients. After adding the copper extension, the reflection coefficient at the resonant frequency was significantly reduced, which reveals that much higher portion of EM energy was confined inside the resonant chamber instead of being reflected. With the coupling improvement and dynamic feedback control during the rewarming, it is expected that our optimized EM resonance system can concentrate higher portion of EM energy in the cavity and be employed for the ultrafast rewarming of cryopreserved materials. On the other hand, the magnetic field induced by the oscillating electric field in the resonance cavity was omitted in the rewarming of CPAs without magnetic nanoparticles in previous trials[16, 24]. As can be seen in the EM distribution (Fig 4E), in addition to the enhanced electric field (the two color slices represent magnitude and the red arrows represent the direction), the associated magnetic field (black arrows) may be utilized potentially to be converted into heat, provided a method to improve the negligible magnetic properties in most cryopreserved biomaterials to interact with the applied oscillating magnetic field.

The effect of embedded MNPs on the EM resonance rewarming of CPA solutions

After cooled by vapor phase nitrogen as described above, the samples were covered by Styrofoam to reduce convection effects, transferred into the center of the resonance chamber, and rewarmed by the optimized EM resonance system. The temperature changes from −130 °C to 0 °C for DPVP with different concentrations of 10nm, 15nm Fe_3O_4 nanoparticles (Fig. 5A) were recorded by the fiber optic thermometer. The onset of devitrification (formation of small ice crystals) may be less lethal to tissues compared to recrystallization (the growth of ice crystals)[32]. For large tissue cryopreservation, it is assumed that relatively slow warming rate should be used initially to avoid fractures or cracks induced by uneven warming. Then the warming should be as rapid as possible to pass through the recrystallization zone. Moreover, an ice free cryopreservation protocol was proposed for tissue preservation in the last decade[33, 34], in which rewarming only happens in the temperature range above the glass transition temperature (around −80 °C). Hence, the entire rewarming temperature range was separated into two sections: −130 °C to −70 °C and −70 °C to 0 °C, and corresponding average rewarming rates were reported (Fig. 5B and C). In this study, we emphasized the rapidity of rewarming during the temperature range −70 °C to 0 °C. Without adding Fe_3O_4 nanoparticles, the average warming rate for DPVP reached 76.0 ± 1.5 °C min^{-1} from −130 °C to −70 °C, and 105.6 ± 6.0 °C min^{-1} from −70 °C to 0 °C using this optimized EM resonance system. To investigate the impact of nanoparticles of different sizes, 10nm and 15nm Fe_3O_4 nanoparticles were added. The MNPs exhibit superparamagnetic properties with size reduced to about 15 nm[35] and superparamagnetic MNPs possess remarkable heating capabilities at lower magnetic fields[36]. Even for the lowest concentration of 0.05 mg Fe mL^{-1} in this study, the rewarming rates in the temperature range −130 °C to −70 °C were increased to 104.9 ± 2.9 °C min^{-1} and 101.9 ± 4.3 °C min^{-1} for solutions with 10 nm and 15 nm Fe_3O_4 nanoparticles,

respectively. In the temperature range from −70 °C to 0 °C, the warming rates were enhanced to 164.4 ± 22.6 °C min^{-1} and 142.3 ± 12.3 °C min^{-1} for solutions with 10 nm and 15 nm Fe_3O_4 nanoparticles, respectively, corresponding to a 61.2% and 39.6% rewarming rate enhancement. Fig. 6A and B show the freeze-warming behavior of DPVP solutions determined by differential scanning calorimetry (DSC). The cooling rates and heating rates for the minuscule sample in DSC were set in agreement with the bulk cryopreserved materials rewarmed by the resonance system. The addition of Fe_3O_4 nanoparticles in DPVP did not change the heat flow during the rewarming. Also, the devitrification phenomena for DPVP with or without Fe_3O_4 nanoparticles were not observed using the rapid warming rates, illustrating that the ultrafast rewarming achieved by the EM resonance rewarming system can prevent severe devitrification or recrystallization.

Fundamentally, the MNPs heat release under oscillating magnetic fields (RF coil heating) are due to several mechanisms of magnetic energy conversion: hysteresis, relaxation rotation of the particles in the fluid (referred to Brownian relaxation) and rotation within the particle (known as Nèel relation)[11]. Magnetic hysteresis can be neglected in the context using superparamagnetic MNPs[37]. Therefore magnetic heat generation is owning to the latter effects which provide energy after displacing the moment of nanoparticles and relaxing back to the equilibrium. The characteristic time for Brownian and Nèel relaxation mechanisms were described by the following equations[38, 39]:

$$\tau_B = \frac{3\eta V_H}{kT}, \tag{2}$$

$$\tau_N = \frac{\tau_0}{2}\sqrt{\pi \frac{kT}{KV}} e^{KV/kT}, \tag{3}$$

where η is the viscosity of the fluid and V_H is the hydrodynamic volume of the particle. K represents the anisotropy constant and V denotes the volume of the particle. The effective

relaxation time accounting for the combination of the two mechanisms and heat generation related to the relaxation are given by[39]:

$$\frac{1}{\tau} = \frac{1}{\tau_B} + \frac{1}{\tau_N} , \quad (4)$$

$$P = \frac{1}{2}\omega\mu_0\chi_0 H^2 \frac{\omega\tau}{1+\omega^2\tau^2} , \quad (5)$$

where ω is the angular frequency of the applied magnetic field and H represents the field magnitude. The effective relaxation time is dominated by the shorter response. For larger particles the Brownian relaxation tends to play a significant role, while Neel relaxation for smaller particles[11].

When taking account of the complex interactions between the oscillating magnetic field and MNPs, the optimal nanoparticle size for different biomedical applications should be different. For the MNPs heating under the oscillating magnetic field created by RF coil (used in hyperthermia study), it is commonly noted that the MNPs enhanced EM heating generation is dependent on the MNP size[40, 41, 42]. The difference can result from the EM field frequency, intensity as well as the pattern of EM field distribution. Also, the magnetization of MNPs is affected by the temperature as can be seen in eq. (1), (2), and has been experimentally tested[42, 43]. The MNPs enhanced heating in cryopreservation (cryogenic temperature as low as −196 °C) is identical to other heating applications such as magnetic hyperthermia which focus the temperature range around 40 °C. Secondly, our resonance system operates at different frequency range (hundreds of MHz versus hundreds of kHz). thirdly, the EM field distribution is distinct to RF coil heating devices which used in hyperthermia or “nanowarming” technique. Thus, the optimum nanoparticle amount and size in our system for cryopreservation cannot be determined by those RF coil heating investigations yet.

As shown in Fig. 5C, rewarmed by this optimized EM resonance, DPVP with 10 nm Fe_3O_4 nanoparticles yielded higher rewarming rates than 15 nm Fe_3O_4 nanoparticles: 164.4 ± 22.6 °C min^{-1} versus 142.3 ± 12.3 °C min^{-1} at 0.05 mg Fe mL^{-1} ($p = 0.15$), 210.1 ± 19.7 °C min^{-1} versus 162.4 ± 3.7 °C min^{-1} at 0.1 mg Fe mL^{-1} ($p < 0.05$), 171.4 ± 2.7 °C min^{-1} versus 145.3 ± 11.0 °C min^{-1} at 0.2 mg Fe mL^{-1} ($p < 0.05$) in the temperature range from −70 °C to 0 °C. The results implied that 10 nm MNPs may be favored from the perspective of EM energy absorption in our system.

The effect of nanoparticles concentration on the rewarming rate was also demonstrated in Fig. 5C for either 10 nm or 15 nm Fe_3O_4 nanoparticles. Each test was repeated for four times. The rewarming rate of DPVP solution embedded with 10 nm Fe_3O_4 nanoparticles at the concentration of 0.1 mg Fe mL^{-1} was 210.1 ± 19.7 °C min^{-1}. significantly more rapid than the lower concentration of 0.05 mg Fe mL^{-1} or higher concentration of 0.2 mg Fe mL^{-1} ($p < 0.05$). The rewarming study of 15nm Fe_3O_4 nanoparticles indicated the similar result. The highest rewarming rate was observed at 0.1 mg Fe mL^{-1} rather than the other two concentrations. The rewarming rates did not progressively increase along with the concentration of Fe_3O_4. We hypothesize that collective behavior between MNPs occurs as the concentration increases but the increasing collective behavior did not contribute to a higher ability to absorb EM energy into heat in the rewarming temperature range in cryopreservation using our EM resonance rewarming method. Invisible ice recrystallization might interact with more concentrated nanoparticles and hinder the heating. In addition, the underlying mechanisms of the increasing inter-particle interactions on the influence of heating efficiency are not well established yet. There are several studies reporting that the heating efficiencies tend to decrease as the concentration of MNPs increases[44, 45, 46] while some experimental studies showed the opposite trend[47, 48]. For the purpose of ultrafast rewarming in

cryopreservation, more experimental findings are needed to get a profound understanding on the EM energy conversion ability in this low temperature range at the applied specific EM frequency. Nevertheless, the small amount but effective Fe_3O_4 nanoparticles in the current work demonstrated beneficial to avoid the potential hazards due to excessive dosage of MNPs.

The efficiency of the EM rewarming

Often, the EM-thermal energy conversion efficiency of the MNPs under the external magnetic field is described as specific absorbance rate (SAR) or referred to as specific loss powers (SLP) in some cases.

$$SAR = \frac{Cm_{total}}{m_{Fe}} \frac{\Delta T}{\Delta t} \tag{6}$$

In most RF coil heating applicators, electric field component is circular along the RF coil used to generate the EM field, while the magnetic field component is perpendicular to the electric field plane. Under the low frequency and for small MNPs, the heating effects induced by possible associated electric filed (i.e. eddy currents) are neglected[41]. Hence, SAR represents the efficiency of magnetic field energy conversion. Commonly, SAR[6, 27, 49, 50] falls in the range of 50–500 W g^{-1}. By improving the design and synthesis of MNPs, SAR[42, 51, 52, 53] can be increased to 1000–4000 W g^{-1}. This level of SAR for RF coil magnetic heating can result in a heating rate of less than 10 °C min^{-1} in the temperature range between 30–50 °C, which is sufficient for biomedical applications in need of only a few temperature increase to release drug[1] or eradicate tumor cells[6]. However, this level of SAR may not be high enough in the context of cryopreservation of large samples, where hundreds of °C min^{-1} or even higher to thousands of °C min^{-1} are preferred. The insufficient energy transfer efficiency leads to the adoption of higher EM source power for RF coil system[8] or other suboptimal EM systems[22]. In the optimized EM resonance rewarming system in this work, both magnetic field and electric filed contribute to the rewarming. An average warming rate of

over 200 °C min^{-1} during the dangerous recrystallization temperature range was achieved for cryopreserved samples with volume up to 20 mL.

Here the contribution of electrical heating and magnetic heating could hardly be differentiated, exact SAR with respect to the MNPs has not been determined yet (if incorporating the electrical heating in the calculation of SAR, SAR would unrealistically turn to over 5000 W g^{-1}). Nevertheless, the power utilization efficiency can be compared with the other studies. To heat the sample in the same order of volume size, RF coil magnetic system[8] adopting over 10 kW achieved an average warming rate of around 120 °C min^{-1}. Another numerical simulation[54] on MNPs based EM heating pointed out 8000 W source power can yield approximately 120 °C min^{-1}. The issue of the ultrahigh source power should be addressed in various EM heating applications where a significant part of energy was not used to heat the target cells/materials but dissipated into heat within the EM generation system or connective circuits, for which an extra cooling[49, 50] system must be assembled to prevent system malfunction. Whereas our optimized EM resonance system only used 500 W. With the dynamic resonance tracking technique, the EM energy transfer efficiency was significantly increase, and the overheating caused by reflected power can be avoided. The experimental results and analysis showed that the system with MNPs not only can obtain higher warming rate, but also convert energy very efficiently.

Post-thawing temperature distribution

Temperature distributions recorded by IR thermometer (Fig. 7A) were analyzed to characterize the temperature gradients after the rewarming. The large temperature difference in DPVP without Fe_3O_4 (Over 30 °C) imply that threatening thermal stresses may occur. The addition of Fe_3O_4, either 10nm or 15nm, notably reduced the inhomogeneity in the final temperature distribution. Here the temperature gradient was calculated as the maximum temperature difference divided by

the distance. As Fig. 7B shows, the temperature gradient for DPVP without MNPs is 2.2 ± 0.41 °C mm^{-1}. The temperature gradients for DPVP with 10nm Fe_3O_4 are lower than those with 15nm Fe_3O_4: 0.83 ± 0.07 °C mm^{-1} versus 1.68± 0.21 °C mm^{-1} at 0.05 mg Fe mL^{-1} ($p < 0.005$); 1.33 ± 0.18 °C mm^{-1} versus 1.78 ± 0.22 °C mm^{-1} at 1 mg Fe mL^{-1} ($p < 0.05$); 1.61 ± 0.28 °C mm^{-1} versus 2.28 ± 0.52 °C mm^{-1} at 0.2 mg Fe mL^{-1} ($p = 0.077$). It was noted that the temperature gradient slightly increased as the concentration of Fe_3O_4, irrespective of the nanoparticle size. The thermal conductivities of the CPAs were determined in the temperature range from −30 °C to 20 °C as shown in Fig. 8A and B. The higher concentration of Fe_3O_4 enhanced the thermal conductivities. Since conduction is the only heat transfer approach within the cryopreserved material for the boundary rewarming technique, a higher thermal conductivity generally increases the uniformity of temperature distribution. Whereas in this study, the enhancement of thermal conductivities was observed as the increase of the concentration of Fe_3O_4, but the improvement in the uniformity was not found. Hence, we assume that the electric and magnetic properties change due to the addition of MNPs altered the interaction between the CPAs and applied EM fields. The nonuniform temperature distribution is primarily due to the EM field distribution within the cryopreserved material. We suppose that with the presence of low dosage MNPs, the temperature uniformity was improved due to the increased thermal conductivity. However, under the illumination of the external EM field, local high intensity fields were induced by the MNPs. As the continuous increasing amount of embedded MNPs, the local fields may exaggerate the temperature non-uniformity related to the EM field distribution.

In the short period time by this optimized rewarming system compared to the traditional boundary heating approach, the heating is dominant by the EM energy conversion instead of conductive heat transfer. The EM field inside the CPAs and the electric properties is more

important than the enhancement of thermal conductivity in determining the uniformity of temperature distribution. The EM resonances from nanoparticles depend on the nature of the nanoparticles, frequency and several other parameters[55, 56]. As for this particular application which involves microwave frequency EM wave and low temperature, the detailed contribution from the MNPs may be clearly understood with more investigations under precisely controlled conditions and specific measurement instruments.

Conclusion

In summary, we developed an optimized EM resonance rewarming system augmented with a dynamical control component for a rapid and uniform rewarming of large cryopreserved materials. With the introduction of Fe_3O_4 nanoparticles, EM energy was exploited at a higher efficiency. The rewarming of the CPA with 10nm Fe_3O_4 at 0.1 mg Fe mL^{-1} showed a significant enhancement in the rate (210.1 °C min^{-1}) and final temperature uniformity (1.33 °C mm^{-1}), which opens another gate to solve the rewarming bottleneck problem in tissue or organ preservation.

This study merely practiced 500 W source power due to the efficient EM energy utilization. Avoiding the difficulty in escalating commercial available RF source power[21], the EM resonance approach is more feasible to scale up for larger biomaterials preservation by controlling the system during the dynamic heating process, maintaining the high energy conversion efficiency. Moreover, RF radiation, the frequency range 30 kHz-300 GHz EM waves including the microwave, was defined a 'possible' human carcinogen (Group 2B) by World Health Organization[57] in 2011, and the classification was not changed[58] at a meeting in 2017. Minimizing radiation power in our closed EM system (the resonance rewarming chamber acts as EM shielding) can be beneficial to avoid the potential risk brought by EM exposure in the open system, such as the high-power RF coil heating device.

Finally, the thermal analysis partly elucidated the contribution of Fe_3O_4 nanoparticles in the cooling and rewarming. To fully understand the quantitative enhancement of embedded MNPs in the EM rewarming and cryopreservation, particularly in separating the effects of improvement in electric field absorption and magnetic field energy utilization, more extensive studies are needed to explore the EM-thermal conversion effects of MNPs in different CPAs in subzero temperature ranges; quantitatively analyze the influences on the magnetic properties and the electric properties, which can facilitate the optimization of the MNPs assisted EM rewarming for tissue or organ preservation.

Figures

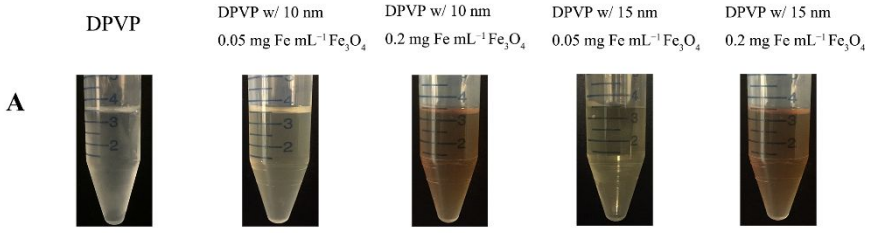

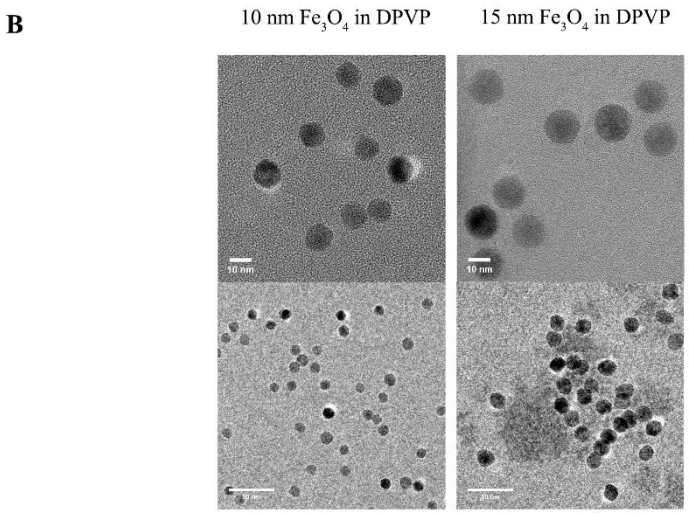

Figure 1. DPVP solutions with 10, 15nm Fe_3O_4 nanoparticles: (A) visual examination of solutions w/ or w/o different Fe_3O_4 concentrations after slow cooling and rapid rewarming; (B) transmission electron microscopy images. Stratified solution after rewarming or nanoparticle aggregations were not observed.

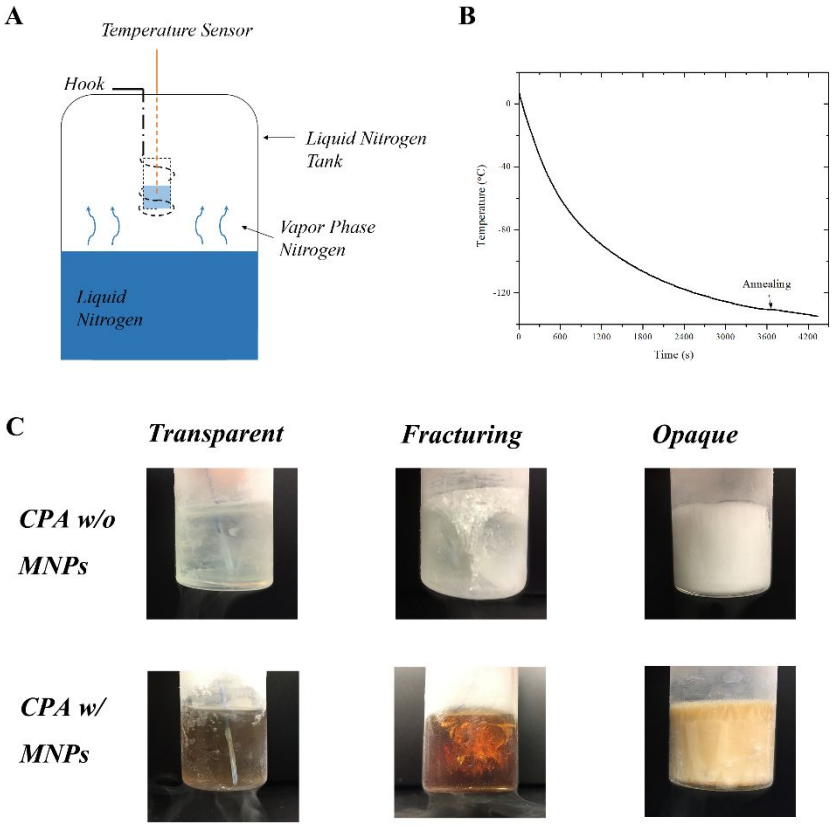

Figure 2. (A) Schematic illustration of the controlled cooling setup. The CPA solutions in holder is hanged by a hook and placed above the surface of liquid nitrogen. The cooling rate could be roughly estimated by adjusting the distance between the CPA and the liquid nitrogen level. (B) A representative temperature change is illustrated using this vapor phase cooling method recorded by thermal sensors. (C) Typical visual images of CPA solutions cooled down to −140 °C. DPVP

w/ or w/o Fe_3O_4 nanoparticles formed transparent solid (left) using the vapor phase cooling method. Cracks (middle) were seen after plunging the bulk DPVP w/ or w/o nanoparticles into liquid nitrogen. Opaque crystalline solid (right) was observed for slowly cooled 5.2 M DMSO, 5.2 M DMSO solution is unable to be vitrified at this low cooling rate.

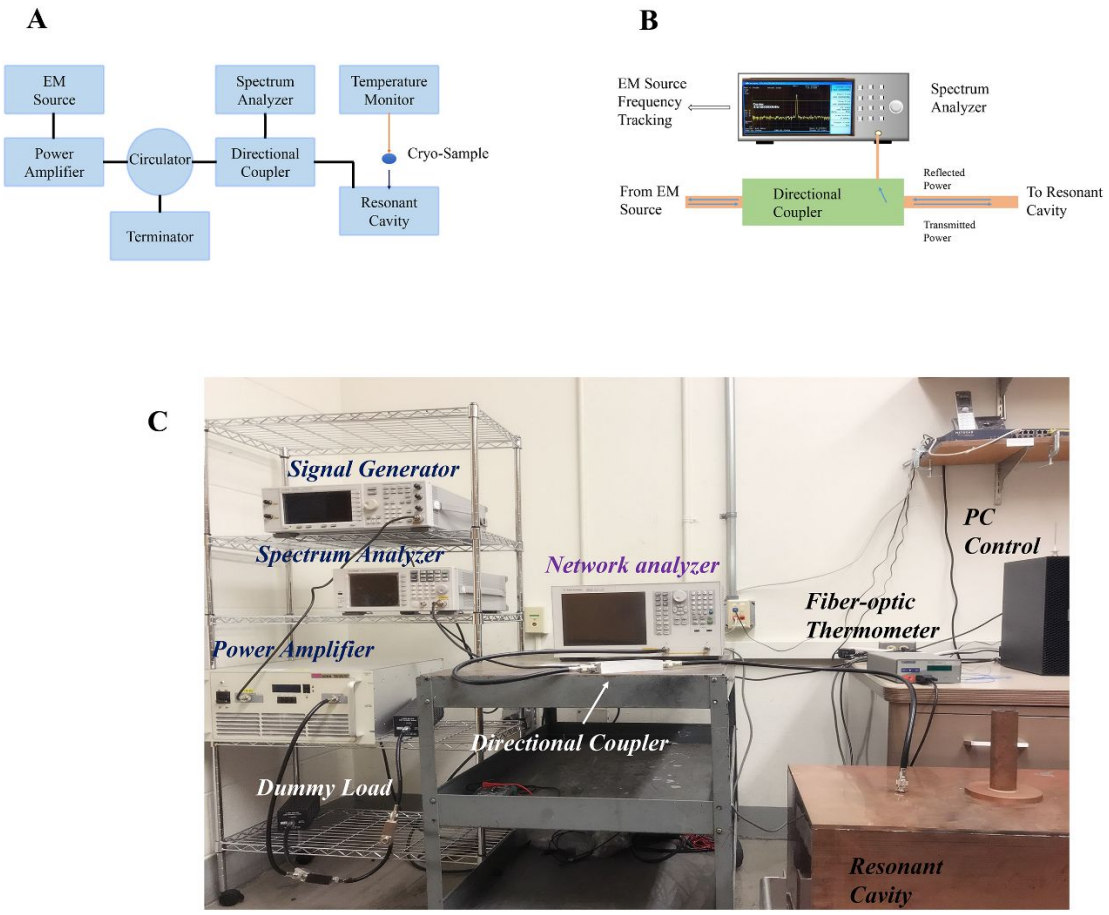

Figure 3. Schematic illustration (A) and photograph (C) of the entire optimized EM resonance system configuration used to achieve the ultrafast rewarming process. The dynamic feedback component (B) consists of a directional coupler and a spectrum analyzer to monitor the reflected

power distribution. The EM source can be adjusted based on the acquired reflected power spectrum accordingly to track the resonance of the EM system.

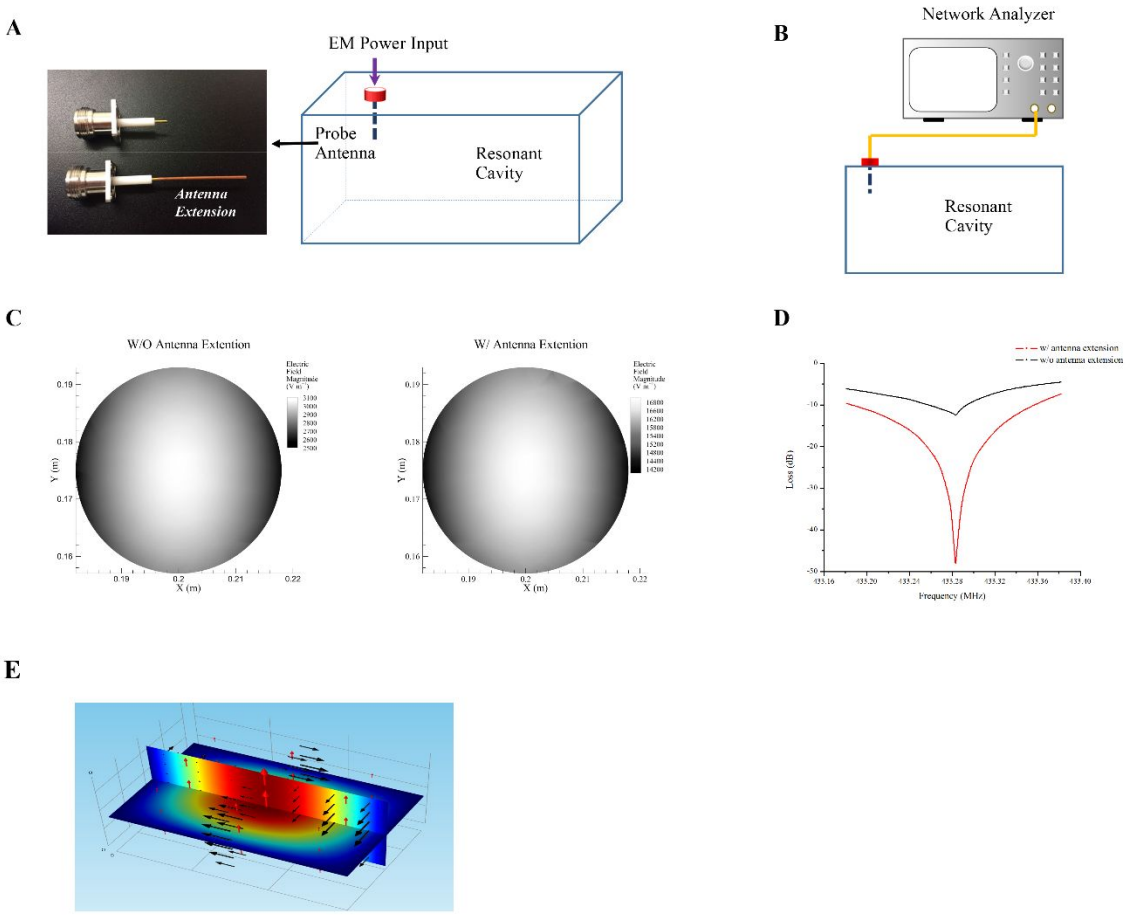

Figure 4. (A) Probe antenna conducting EM energy into the resonance chamber. (B) Schematic of the determination of the cavity resonance state using a network analyzer. After the addition of copper extension, a five-fold increase in the simulated electric field magnitude was seen in the center of chamber (C) where the cryopreserved material was located; the experimentally determined reflection coefficient (D) was minimized indicating much less portion of energy reflected from the resonant cavity back to the source. (E) EM field distribution inside the resonant

cavity. Color slices represent the electric field magnitude. Red arrow and black arrows indicate the direction of electric and magnetic fields, respectively.

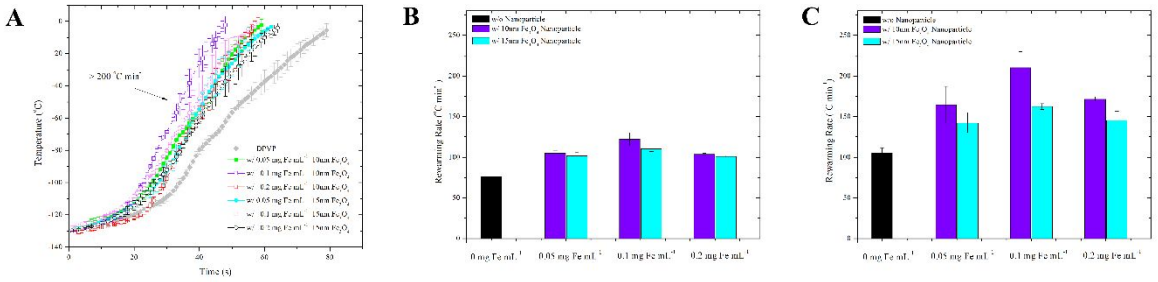

Figure 5. The rewarming of CPA solutions with embedded Fe_3O_4 nanoparticles using the EM resonance system. (A) Temperature change of the CPA solutions during the rewarming process. Average value of temperature versus time was given based on four measurements. Average warming rates were determined for the rewarming temperature range −130 °C to −70 °C (B) and −70 °C to 0 °C (C). The error bars represented the standard deviation. Each test was repeated for four times.

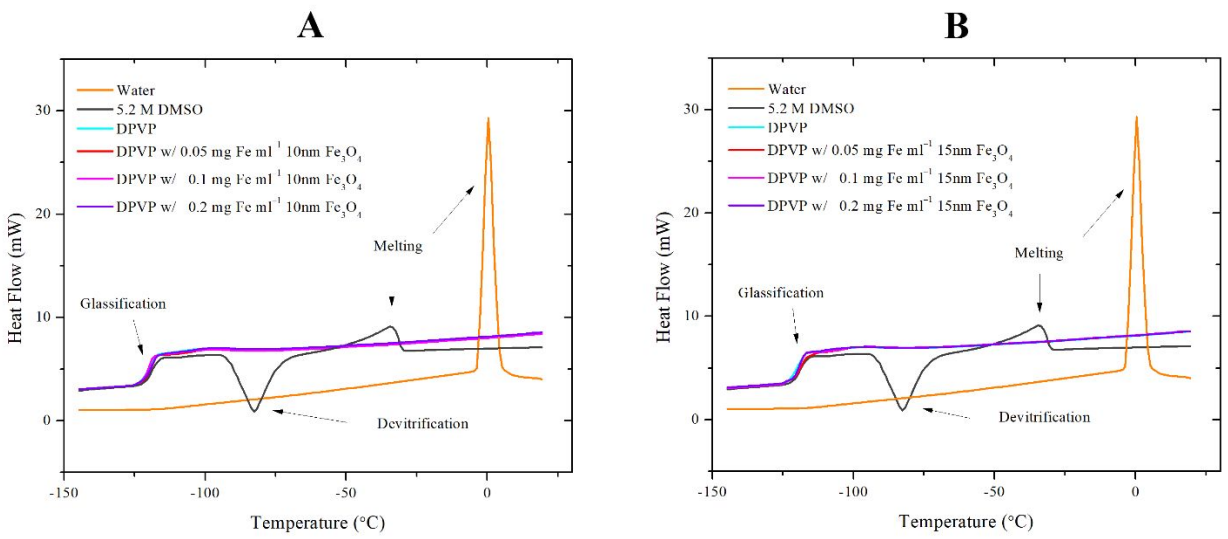

Figure 6. Freeze-warming behavior of CPA solutions with 10nm Fe_3O_4 nanoparticles (A) and 15nm Fe_3O_4 nanoparticles (B). The devitrification, melting of 5.2 M dimethyl sulfoxide (DMSO) occurred at a warming rate 100 °C min^{-1}. Whereas the apparent recrystallization of DPVP with Fe_3O_4 nanoparticles was not observed using the same protocol. The cooling and heating rates were set in accordance with the bulk cryopreserved materials in the EM resonance rewarming.

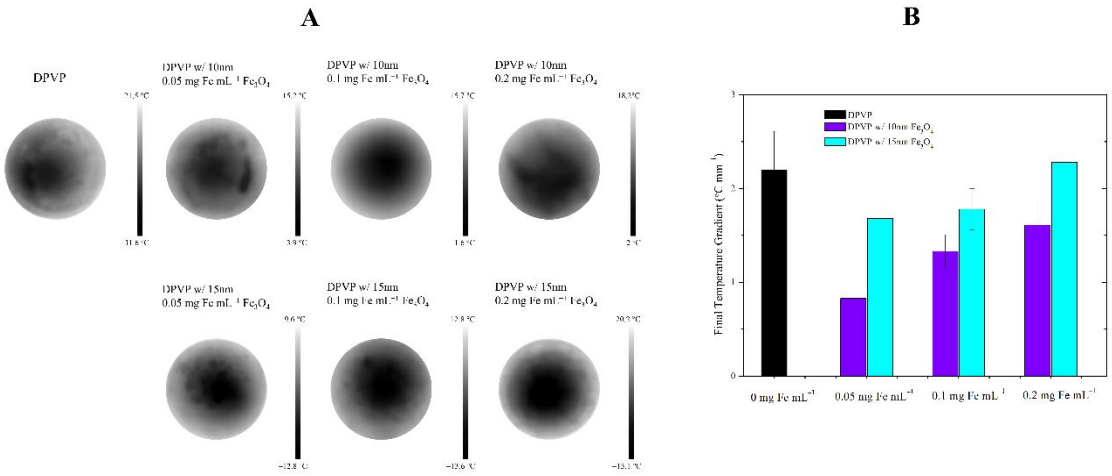

Figure 7. The post-rewarming of CPA solutions with embedded Fe_3O_4 nanoparticles using the EM resonance system. (A) Surface temperature distribution. (B) The temperature gradients were calculated as the maximum temperature difference divided by the distance. Mean values ± standard deviations were determined based on four measurements.

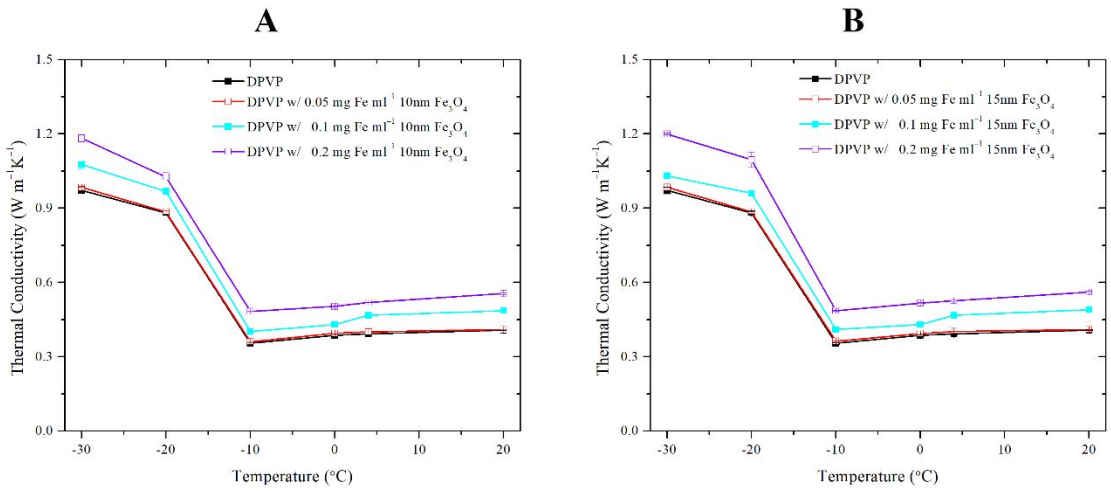

Figure 8. Thermal conductivities of CPA solution with 10nm Fe_3O_4 nanoparticles (A) and 15nm Fe_3O_4 nanoparticles (B). Mean values ± standard deviations were determined based on four measurements.

Author Contributions

J. Pan and D. Gao conceived the project. J. Pan and M. Chen designed and optimized the experiment system. J. Pan and S. Ren performed the rewarming experiments and obtained the temperature data. S. Ren performed the thermal analysis. P. Sekar manufactured the thermal sensor and performed the thermal conductivity measurement. J. Peng and J. Pan designed the cooling protocol and performed the vitrification experiment. J. Pan prepared the manuscript. Z. Shu, W. Ding and G. Zhao revised the manuscript. All authors reviewed and approved the submitted manuscript.

Acknowledgement

We thank the molecular Analysis Facility (MAF) for their work in TEM sample preparation and image acquisition.

Reference

1. Hayashi K, Ono K, Suzuki H, Sawada M, Moriya M, Sakamoto W*, et al.* High-Frequency, Magnetic-Field-Responsive Drug Release from Magnetic Nanoparticle/Organic Hybrid Based on Hyperthermic Effect. *Acs Appl Mater Inter* 2010, **2**(7)**:** 1903-1911.

2. Kumar CSSR, Mohammad F. Magnetic nanomaterials for hyperthermia-based therapy and controlled drug delivery. *Adv Drug Deliver Rev* 2011, **63**(9)**:** 789-808.

3. Liong M, Lu J, Kovochich M, Xia T, Ruehm SG, Nel AE*, et al.* Multifunctional inorganic nanoparticles for imaging, targeting, and drug delivery. *Acs Nano* 2008, **2**(5)**:** 889-896.

4. Sun C, Lee JSH, Zhang MQ. Magnetic nanoparticles in MR imaging and drug delivery. *Adv Drug Deliver Rev* 2008, **60**(11)**:** 1252-1265.

5. Park JH, von Maltzahn G, Xu MJ, Fogal V, Kotamraju VR, Ruoslahti E*, et al.* Cooperative nanomaterial system to sensitize, target, and treat tumors. *P Natl Acad Sci USA* 2010, **107**(3)**:** 981-986.

6. Johannsen M, Gneueckow U, Thiesen B, Taymoorian K, Cho CH, Waldofner N*, et al.* Thermotherapy of prostate cancer using magnetic nanoparticles: Feasibility, imaging, and three-dimensional temperature distribution. *Eur Urol* 2007, **52**(6)**:** 1653-1662.

7. Etheridge ML, Xu Y, Rott L, Choi J, Glasmacher B, Bischof JC. RF heating of magnetic nanoparticles improves the thawing of cryopreserved biomaterials. *Tehnology* 2014, **2**(3)**:** 229-242.

8. Manuchehrabadi N, Gao Z, Zhang JJ, Ring HL, Shao Q, Liu F*, et al.* Improved tissue cryopreservation using inductive heating of magnetic nanoparticles. *Sci Transl Med* 2017, **9**(379).

9. Giwa S, Lewis JK, Alvarez L, Langer R, Roth AE, Church GM*, et al.* The promise of organ and tissue preservation to transform medicine. *Nat Biotechnol* 2017, **35**(6)**:** 530-542.

10. Scott KL, Lecak J, Acker JP. Biopreservation of red blood cells: Past, present, and future. *Transfus Med Rev* 2005, **19**(2)**:** 127-142.

11. Broxmeyer HE, Srour EF, Hangoc G, Cooper S, Anderson SA, Bodine DM. High-efficiency recovery of functional hematopoietic progenitor and stem cells from human cord blood cryopreserved for 15 years. *P Natl Acad Sci USA* 2003, **100**(2)**:** 645-650.

12. Henry MA, Noiles EE, Gao DY, Mazur P, Critser JK. Cryopreservation of Human Spermatozoa .4. The Effects of Cooling Rate and Warming Rate on the Maintenance of Motility, Plasma-Membrane Integrity, and Mitochondrial-Function. *Fertil Steril* 1993, **60**(5)**:** 911-918.

13. Bernard A, Fuller BJ. Cryopreservation of human oocytes: A review of current problems and perspectives. *Hum Reprod Update* 1996, **2**(3)**:** 193-207.

14. Fahy GM, MacFarlane DR, Angell CA, Meryman HT. Vitrification as an approach to cryopreservation. *Cryobiology* 1984, **21**(4)**:** 407-426.

15. Evans S, Rachman MJ, Pegg DE. Design of a UHF applicator for rewarming of cryopreserved biomaterials. *Ieee T Bio-Med Eng* 1992, **39**(3)**:** 217-225.

16. Robinson MP, Pegg DE. Rapid electromagnetic warming of cells and tissues. *IEEE transactions on bio-medical engineering* 1999, **46**(12)**:** 1413-1425.

17. Evans S, Penfold J. Thermal runaway in electromagnetic heating, with application to the reheating of cryopreserved biomaterials. *J Microwave Power Ee* 1993, **28**(2)**:** 84-92.

18. Rodriguez-Luccioni HL, Latorre-Esteves M, Mendez-Vega J, Soto O, Rodriguez AR, Rinaldi C*, et al.* Enhanced reduction in cell viability by hyperthermia induced by magnetic nanoparticles. *Int J Nanomed* 2011, **6:** 373-380.

19. Jordan A, Wust P, Scholz R, Tesche B, Fahling H, Mitrovics T*, et al.* Cellular uptake of magnetic fluid particles and their effects on human adenocarcinoma cells exposed to AC magnetic fields in vitro. *Int J Hyperther* 1996, **12**(6)**:** 705-722.

20. Brigger I, Dubernet C, Couvreur P. Nanoparticles in cancer therapy and diagnosis. *Adv Drug Deliv Rev* 2002, **54**(5)**:** 631-651.

21. Dutz S, Hergt R. Magnetic particle hyperthermia-a promising tumour therapy? *Nanotechnology* 2014, **25**(45).

22. Wang T, Zhao G, Deng ZS, Gao C, Cao YX, Gao DY. Theoretical investigation of a novel microwave antenna aided cryovial for rapid and uniform rewarming of frozen cryoprotective agent solutions. *Appl Therm Eng* 2015, **89:** 968-977.

23. Pan J, Shu Z, Ren S, Gao D. Determination of dielectric properties of cryoprotective agent solutions with a resonant cavity for the electromagnetic rewarming in cryopreservation. *Biopreserv Biobank* 2017.

24. Luo DW, Yu C, He LQ, Lu CC, Gao DY. Development of a single mode electromagnetic resonant cavity for rewarming of cryopreserved biomaterials. *Cryobiology* 2006, **53**(2)**:** 288-293.

25. Gao D, Critser JK. Mechanisms of cryoinjury in living cells. *ILAR journal* 2000, **41**(4)**:** 187-196.

26. Liang XM, Sekar PK, Zhao G, Zhou XM, Shu ZQ, Huang Z*, et al.* High accuracy thermal conductivity measurement of aqueous cryoprotective agents and semi-rigid biological tissues using a microfabricated thermal sensor. *Sci Rep-Uk* 2015, **5**.

27. Jeon S, Hurley KR, Bischof JC, Haynes CL, Hogan CJ. Quantifying intra- and extracellular aggregation of iron oxide nanoparticles and its influence on specific absorption rate. *Nanoscale* 2016, **8**(35)**:** 16053-16064.

28. Boutron P, Kaufmann A. Stability of the amorphous state in the system water--glycerol--dimethylsulfoxide. *Cryobiology* 1978, **15**(1)**:** 93-108.

29. Fahy GM, Wowk B, Wu J, Paynter S. Improved vitrification solutions based on the predictability of vitrification solution toxicity. *Cryobiology* 2004, **48**(3)**:** 365-365.

30. Huang HS, Choi JK, Rao W, Zhao ST, Agarwal P, Zhao G*, et al.* Alginate Hydrogel Microencapsulation Inhibits Devitrification and Enables Large-Volume Low-CPA Cell Vitrification. *Adv Funct Mater* 2015, **25**(44)**:** 6839-6850.

31. Zhao G, Fu JP. Microfluidics for cryopreservation. *Biotechnol Adv* 2017, **35**(2)**:** 323-336.

32. Fahy GM, Wowk B. Cryopreservation and freeze-drying protocols. In: Wolkers WF, Oldenhof H (eds). Springer: New York, 2015, pp 21-82.

33. Brockbank KGM, Wright GJ, Greene ED, Chen ZZ, Schenke-Layland K. Allogeneic Heart Valve Storage Above the Glass Transition at-80 degrees C. *Ann Thorac Surg* 2011, **91**(6)**:** 1829-1835.

34. Lisy M, Pennecke J, Brockbank KGM, Fritze O, Schleicher M, Schenke-Layland K*, et al.* The performance of ice-free cryopreserved heart valve allografts in an orthotopic pulmonary sheep model. *Biomaterials* 2010, **31**(20)**:** 5306-5311.

35. Deatsch AE, Evans BA. Heating efficiency in magnetic nanoparticle hyperthermia. *J Magn Magn Mater* 2014, **354:** 163-172.

36. Pankhurst QA, Connolly J, Jones SK, Dobson J. Applications of magnetic nanoparticles in biomedicine. *J Phys D Appl Phys* 2003, **36**(13)**:** R167-R181.

37. Tanaka K, Ito A, Kobayashi T, Kawamura T, Shimada S, Matsumoto K*, et al.* Cancer immunotherapy using hyperthermia with magnetic nanoparticles and dendritic cells. *J Biotechnol* 2005, **118:** S73-S73.

38. Brown WF. Thermal Fluctuations of a Single-Domain Particle. *Phys Rev* 1963, **130**(5)**:** 1677-+.

39. Rosensweig RE. Heating magnetic fluid with alternating magnetic field. *J Magn Magn Mater* 2002, **252**(1-3)**:** 370-374.

40. Gonzales-Weimuller M, Zeisberger M, Krishnan KM. Size-dependant heating rates of iron oxide nanoparticles for magnetic fluid hyperthermia. *J Magn Magn Mater* 2009, **321**(13)**:** 1947-1950.

41. Kalambur VS, Han B, Hammer BE, Shield TW, Bischof JC. In vitro characterization of movement, heating and visualization of magnetic nanoparticles for biomedical applications. *Nanotechnology* 2005, **16**(8)**:** 1221-1233.

42. Ho D, Sun XL, Sun SH. Monodisperse Magnetic Nanoparticles for Theranostic Applications. *Accounts Chem Res* 2011, **44**(10)**:** 875-882.

43. Blanco-Mantecon M, O'Grady K. Interaction and size effects in magnetic nanoparticles. *J Magn Magn Mater* 2006, **296**(2)**:** 124-133.

44. Pineiro-Redondo Y, Banobre-Lopez M, Pardinas-Blanco I, Goya G, Lopez-Quintela MA, Rivas J. The influence of colloidal parameters on the specific power absorption of PAA-coated magnetite nanoparticles. *Nanoscale Res Lett* 2011, **6**.

45. Wang XM, Gu HC, Yang ZQ. The heating effect of magnetic fluids in an alternating magnetic field. *J Magn Magn Mater* 2005, **293**(1)**:** 334-340.

46. Urtizberea A, Natividad E, Arizaga A, Castro M, Mediano A. Specific Absorption Rates and Magnetic Properties of Ferrofluids with Interaction Effects at Low Concentrations. *J Phys Chem C* 2010, **114**(11)**:** 4916-4922.

47. Dennis CL, Jackson AJ, Borchers JA, Ivkov R, Foreman AR, Lau JW*, et al.* The influence of collective behavior on the magnetic and heating properties of iron oxide nanoparticles. *J Appl Phys* 2008, **103**(7).

48. Verges MA, Costo R, Roca AG, Marco JF, Goya GF, Serna CJ*, et al.* Uniform and water stable magnetite nanoparticles with diameters around the monodomain-multidomain limit. *J Phys D Appl Phys* 2008, **41**(13).

49. DeNardo SJ, DeNardo GL, Natarajan A, Miers LA, Foreman AR, Gruettner C*, et al.* Thermal dosimetry predictive of efficacy of In-111-ChL6 nanoparticle AMF-induced thermoablative therapy for human breast cancer in mice. *J Nucl Med* 2007, **48**(3)**:** 437-444.

50. Creixell M, Bohorquez AC, Torres-Lugo M, Rinaldi C. EGFR-Targeted Magnetic Nanoparticle Heaters Kill Cancer Cells without a Perceptible Temperature Rise. *Acs Nano* 2011, **5**(9)**:** 7124-7129.

51. Lartigue L, Hugounenq P, Alloyeau D, Clarke SP, Levy M, Bacri JC*, et al.* Cooperative Organization in Iron Oxide Multi-Core Nanoparticles Potentiates Their Efficiency as Heating Mediators and MRI Contrast Agents. *Acs Nano* 2012, **6**(12)**:** 10935-10949.

52. Guardia P, Di Corato R, Lartigue L, Wilhelm C, Espinosa A, Garcia-Hernandez M*, et al.* Water-Soluble Iron Oxide Nanocubes with High Values of Specific Absorption Rate for Cancer Cell Hyperthermia Treatment. *Acs Nano* 2012, **6**(4)**:** 3080-3091.

53. Lee JH, Jang JT, Choi JS, Moon SH, Noh SH, Kim JW*, et al.* Exchange-coupled magnetic nanoparticles for efficient heat induction. *Nat Nanotechnol* 2011, **6**(7)**:** 418-422.

54. Wang T, Zhao G, Liang XM, Xu YP, Li Y, Tang HY*, et al.* Numerical simulation of the effect of superparamagnetic nanoparticles on microwave rewarming of cryopreserved tissues. *Cryobiology* 2014, **68**(2)**:** 234-243.

55. Kocifaj M, Klačka, J. , Kundracik, F., Videen G. Charge‐induced electromagnetic resonances in nanoparticles. *Annal der Phys* 2015, **527:** 765-769.

56. Kundracik F, Kocifaj M, Videen G, Klacka J. Effect of charged-particle surface excitations on near-field optics. *Applied optics* 2015, **54**(22)**:** 6674-6681.

57. Baan R, Grosse Y, Lauby-Secretan B, El Ghissassi F, Bouvard V, Benbrahim-Tallaa L*, et al.* Carcinogenicity of radiofrequency electromagnetic fields. *Lancet Oncol* 2011, **12**(7)**:** 624-626.

58. Hardell L. World Health Organization, radiofrequency radiation and health - a hard nut to crack (Review). *Int J Oncol* 2017, **51**(2)**:** 405-413.

Competing Interests

The authors declare no competting interests.

TOC Graphic: EM Cavity Resonance rewarming of nanoparticle embedded cryopreserved solution

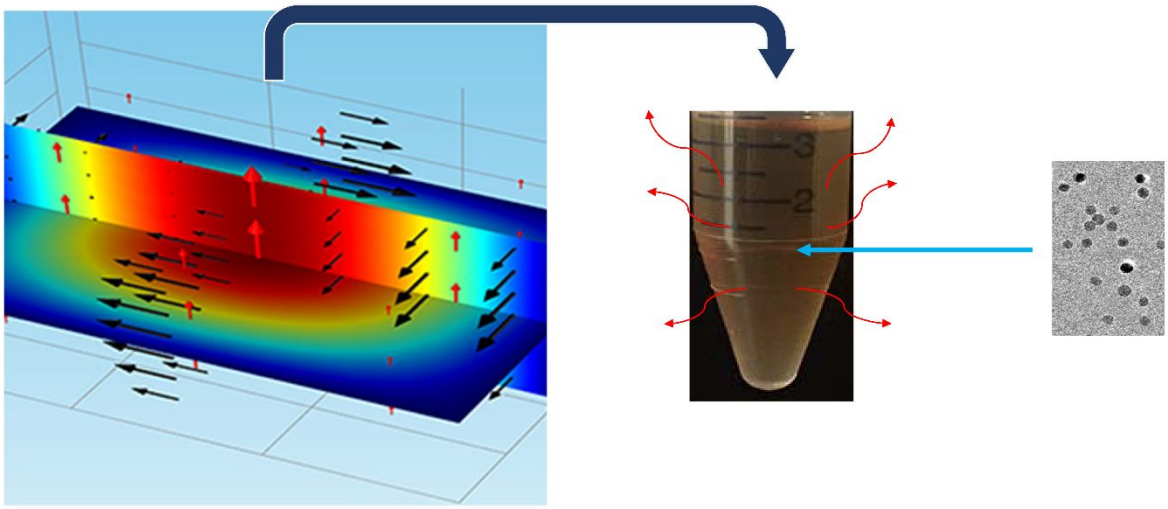

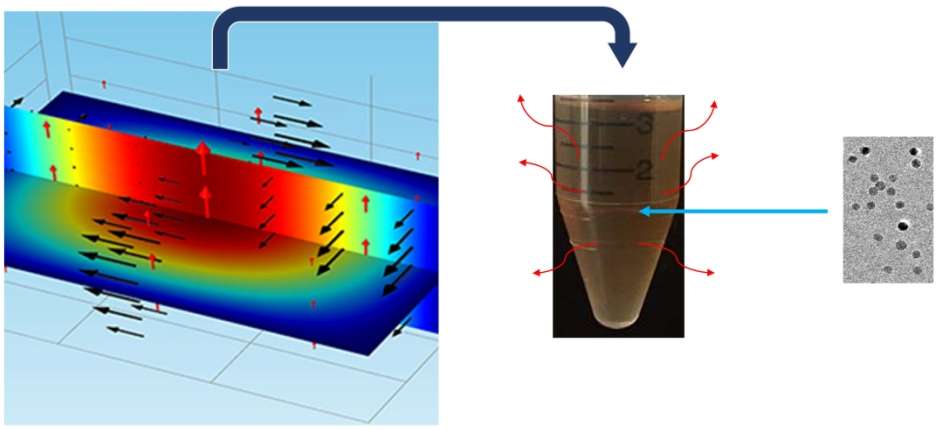

EM Cavity Resonance rewarming of nanoparticle embedded cryopreserved solution

235x119mm (300 x 300 DPI)